MIL-101-NH$_2$(Fe)-Coated Nylon Microfibers for Immobilized Photocatalysts in RhB and Cr(VI) Removal

Munchan Kang, Sung Ho Yu, Kyung-Youl Baek, Myung Mo Sung, and Sangho Cho*

Read Online

ACCESS | Metrics & More | Article Recommendations | SI Supporting Information

ABSTRACT: MIL-101-NH$_2$(Fe) is one of the effective photocatalytic metal−organic frameworks (MOFs) working under visible light. However, its powder-type form inhibits reusability in practical applications. In this study, we immobilized MIL-101-NH$_2$(Fe) on a polymeric microfiber mesh to improve reusability while minimizing the loss of catalytic performance. To overcome the lack of surface functionality of the nylon fibers, an atomic layer deposition Al$_2$O$_3$ layer and NH$_2$-BDC linker were introduced to facilitate uniform coating of the MOF on the fiber surface. The reactions of the metal precursor to the nylon substrate and NH$_2$-BDC ligand of the MOF allow chemical bonding from the core to the shell of the entire hybrid catalytic materials. The resulting fiber-immobilized MOFs (Nylon@Al$_2$O$_3$@MOF) demonstrated high photocatalytic performance in the removal of RhB and Cr(VI) as representatives of organic dyes and heavy metals, respectively, while retaining over 85% of its efficiency after five cycles.
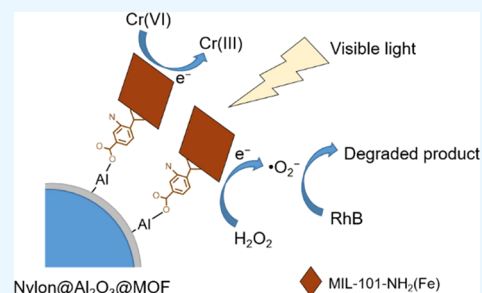
INTRODUCTION

Population growth and industrial development have accompanied a threat to human health arising from organic pollutants and heavy metals in water.[1−3] To mitigate this problem, a variety of strategies have been explored including ion exchange, adsorption, membrane filtration, and chemical/photocatalysis.[4,5] Among these various methods, heterogeneous photocatalysis has emerged as a promising option in the point of minimization of chemical usage and utilization of solar energy for the reactions to occur.[6] However, conventional photocatalysts such as TiO$_2$, CdS, SnS$_2$, and Ag$_2$S have limited absorption in the ultraviolet range owing to their large bandgaps.[7,8]

Metal−organic frameworks (MOFs) have gained attention as photocatalysts due to their desirable topology, high surface and interface area, and the ability to easily tailor functionalities.[9−14] Especially, Fe-based MOFs consisting of Fe−O clusters have emerged as superior photocatalysts with high catalytic activity and stability in organic solvents.[15−17] The originally ultraviolet-active Fe-based MOFs can have their optical properties modulated by the introduction of amine-functionalized organic ligands. This results in a reduced band gap of MOFs, making them activated under visible light irradiation due to the enhanced electron-donating ability of the ligand.[18,19]

Unfortunately, MOFs, like other powder-form catalysts, face a significant challenge with recyclability. The inevitable loss of nano-/micro-sized crystals occurs during a repetition of the filtering and washing process, which limits their practical applications.[20,21] To address this issue, researchers have explored immobilizing photocatalysts by using various supporting materials to form composites, mixed membranes, and thin films.[22−26] For high-efficiency immobilized photocatalysts, supporting materials must possess properties such as a large specific surface area, favorable photoelectric separation, and chemical inertness.[27,28]

In this study, we developed immobilized photocatalytic materials by growing MOFs on the surface of the polymeric fibers mesh. The lightweight and large surface area of the fiber mesh make it a suitable candidate for use as a photocatalytic supporting matrix with easy control of size and shape. Surface immobilization of MOFs offers high efficiency in the photocatalytic reactions by avoiding supporting material-induced light hindrance and dormant surface effects in composite forms. However, the limited surface reactive site on polymeric fibers impedes the surface growth of MOFs. To overcome this, we introduced a thin metal oxide layer on the polymeric fiber, which enhances the growth and adhesion of MOFs to the fiber by facilitating the reaction of the ligand with the surface metal site.[29,30] Among many thin-film formation techniques, atomic layer deposition (ALD) shows promise in creating highly uniform thin films due to the advantages of free solvent and good step coverage.[31,32] Especially, gas-phase ALD precursors could penetrate the free volume of polymer and form a metal oxide-polymer hybrid subsurface region.[33−35] The boundaryless-hybrid layer can prevent delamination of the

ALD layer from the polymer substrate under mechanical strain.[35]

Herein, we chose MIL-101-NH$_2$(Fe) as a photocatalytic MOF and nylon microfiber mesh as a supporting material to fabricate an immobilized MOF photocatalyst. Nylon was selected for its easy infiltration of ALD precursors, which enhances adhesion between the polymer substrate and metal oxide layer.[34] MIL-101-NH$_2$(Fe), consisting of Fe−O clusters and amine-functionalized carboxylic acid ligands, exhibits good photocatalytic activity under visible light irradiation.[36] By employing a two-step growth process involving ligand seed layer and solvothermal MOF growth, we were able to induce surface-initiated MOF growth and successfully coat the microfibers with MOFs. Finally, we evaluated the photocatalytic activity and reusability of this immobilized photocatalyst for the removal of RhB and Cr(VI) as model organic pollutants and heavy metals, respectively.

■ EXPERIMENTAL SECTION

Materials. All reagents were used directly without further purification. Iron chloride hexahydrate (FeCl$_3$·6H$_2$O), 2-aminoterephthalic acid (NH$_2$-BDC, 99%), trimethylalumium (TMA, 99%), acetic acid (AcOH, 97%), rhodamine B (RhB), potassium dichromate (K$_2$Cr$_2$O$_7$, 99%), 1,5-Diphenylcarbazide (DPC, 99%) were purchased from Sigma-Aldrich. N,N-dimethylformamide (DMF, 98%) was purchased from Daejung Chemicals. Nylon microfiber meshes (Figure S1a) with a fiber diameter ranging from 40 to 60 μm were purchased from APEC (South Korea).

Preparation of the MIL-101-NH$_2$(Fe) Powder. MIL-101-NH$_2$ powder was synthesized by a solvothermal method with a slight modification, as previously reported.[37] First, 1.1 g of FeCl$_3$·6H$_2$O and 0.72 g of NH$_2$-BDC were dissolved in 45 mL of DMF under ultrasonication. Then, 1.8 mL of acetic acid was added as a mineralizing agent.[38] The resulting solution was sealed in a 100 mL Teflon-lined autoclave and heated at 120 °C for 24 h. Finally, the brown MIL-101-NH$_2$ powder was obtained by centrifugation at 8000 rpm, washed three times with DMF and ethanol, and dried under vacuum at 90 °C overnight.

Preparation of Nylon@Al$_2$O$_3$. Al$_2$O$_3$ was deposited onto the surface of nylon microfibers using a custom-built hot-wall viscous-flow ALD reactor. The deposition process involved repeated cycles of TMA dosing, Ar purge, H$_2$O dosing, and Ar purge with the nylon microfibers at 120 °C, resulting in a conformal coating of Al$_2$O$_3$ on the microfibers (Nylon@Al$_2$O$_3$). Silicon wafers with 2 nm native oxide in 1 cm^2 size were also placed alongside the nylon microfibers inside the chamber to measure the thickness of the Al$_2$O$_3$ film under the same ALD conditions.

Preparation of Nylon@Al$_2$O$_3$@MIL-101-NH$_2$(Fe). MIL-101-NH$_2$ was grown on the surface of Nylon@Al$_2$O$_3$ via a two-step seeding growth method.[29,30] In the first step for the formation of a seed layer, as-prepared 1 g of Nylon@Al$_2$O$_3$ in 1 cm^2 size was fully soaked in NH$_2$-BDC solution (0.72 g in 30 mL DI water). Then, the mixture was transferred to a 100 mL Teflon-lined autoclave and heated at 120 °C for 24 h. Afterward, the fiber samples were washed with water and dried under vacuum at 60 °C for 4 h (Nylon@Al$_2$O$_3$-BDC). In the second step for MOF growth, as-prepared Nylon@Al$_2$O$_3$-BDC was soaked in the precursor solution prepared using the same recipe depicted as the preparation of MIL-101-NH$_2$(Fe) and heated in the 100 mL autoclave at 120 °C for 24 h. The

resulting Nylon@Al$_2$O$_3$@MOF was washed three times with DMF and anhydrous ethanol and soaked in anhydrous ethanol for a day before drying under vacuum at 90 °C overnight. The thickness of the MOF layer is dependent on factors such as precursor concentration, reaction time, and temperature.

Nylon@MOF was prepared with the same recipe using a bare nylon fiber as a control sample to access the effect of the Al$_2$O$_3$ layer. Nylon@Al$_2$O$_3$@MOF_no seeding was prepared with the same recipe except for the seeding process as a control sample to figure out the effect of the NH$_2$-BDC seeding.

Photocatalytic Experiment. The photocatalytic activity of Nylon@Al$_2$O$_3$@MIL-101-NH$_2$ was assessed by monitoring the concentration change of RhB and Cr(VI) under visible (white) light irradiation. The experiment was conducted at room temperature in a 100 mL beaker consisting of either 60 mL of 50 ppm RhB solution or 5 ppm Cr(VI) solution with 15 mg of MIL-101-NH$_2$ powder or 1 g of Nylon@Al$_2$O$_3$@MIL-101-NH$_2$. The pH values of the samples were adjusted with 0.5 M H$_2$SO$_{4(aq)}$ or NaOH$_{(aq)}$. After stirring for 60 min in dark to reach adsorption−desorption equilibrium, 1.5 mL of 35% H$_2$O$_{2(aq)}$ was added, and visible light was illuminated using a 150 W halogen lamp (Philps) at a distance of 10 cm from the solution (Figure S2).

We monitored Cr(VI) concentration at different time intervals using the DPC method.[39] The reduction of Cr(VI) was detected by the formation of a purple color peaked at 540 nm when hexavalent chromium reacts with 1,5-Diphenylcarbohydrazide in an acidic medium. RhB concentration was determined by measuring UV−vis absorbance at 553 nm using a UV−vis spectrophotometer. Each experiment was repeated three times, and the average value was used for the calculation of the reduction rate constant k, which was determined using pseudo-first-order rate expression given in eq 1.

$$-\ln(C_t/C_0) = kt \qquad (1)$$

To evaluate the recyclability of Nylon@Al$_2$O$_3$@MOF, the rate constants k for RhB degradation and Cr(VI) reduction were measured up to five cycles. For regeneration of the catalyst, Nylon@Al$_2$O$_3$@MOF was soaked in ethanol at room temperature after each cycle.

Characterizations. The surface morphologies of samples were analyzed by field-emission scanning electron microscopy (FE-SEM, Inspect F50, FEI) with energy dispersive spectroscopy (EDS) equipment. Prior to SEM imaging, Pt was sputter-coated onto the prepared samples with a thin layer (5−10 nm). We also obtain cross-section images of Nylon@Al$_2$O$_3$ and Nylon@Al$_2$O$_3$@MOF samples through a transmission electron microscope (TEM, Tecnai F20 G2, FEI) after microtoming. X-ray photoelectron spectroscopy (XPS) analyses were conducted with an electron spectrometer (Nexsa, Thermo Scientific). The XPS spectra were calibrated using the C 1s peak at 284.8 eV. Fourier transform infrared (FT-IR) spectra were carried out using an FT-IR spectrometer (Nicolet iS10, Thermo Scientific). X-ray diffraction (XRD) patterns of Nylon, Nylon@Al$_2$O$_3$, Nylon@Al$_2$O$_3$@MOF, and MOF powder were performed on a diffractometer (D/MAX2200, Bruker). The loading ratios of MOFs within the coated-nylon fiber were calculated by the difference in mass residue obtained from thermogravimetric analysis (TGA, Q-50, TA instrument).

■ RESULTS AND DISCUSSION

Figure 1 illustrates the process of preparing an MOF-coated nylon microfiber. Initially, a nanometer-thin Al$_2$O$_3$ layer was
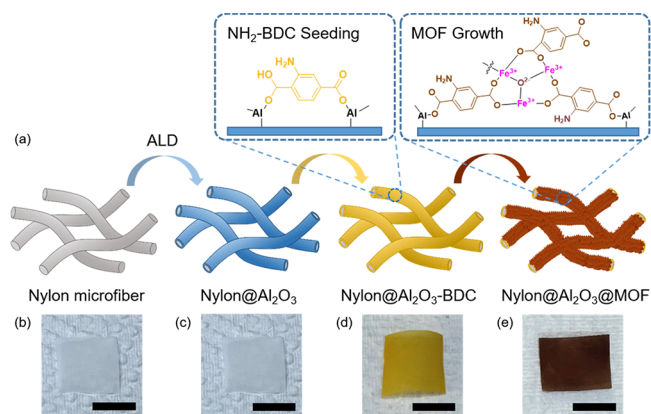
Figure 1. (a) Schematic illustration of the preparation of a MIL-101-NH$_2$(Fe)-coated nylon microfiber (Nylon@Al$_2$O$_3$@MOF). Photo images of (b) nylon microfiber mesh, (c) Nylon@Al$_2$O$_3$, (d) Nylon@Al$_2$O$_3$-BDC, and (e) Nylon@Al$_2$O$_3$@MOF. Scale bar: 1 cm. (Photos were taken by M. Kang).

deposited on the surface of the nylon microfiber mesh using ALD to obtain Nylon@Al$_2$O$_3$. The cross-sectional TEM image (Figure 2e) shows that the sequential exposure of aluminum
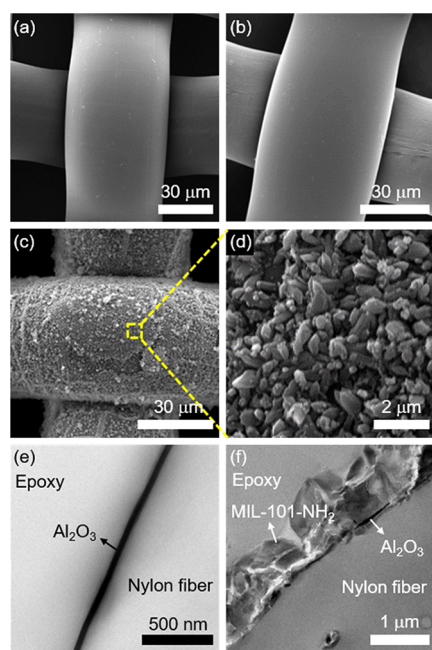

Figure 2. SEM images of (a) nylon microfiber, (b) Nylon@Al$_2$O$_3$, (c) Nylon@Al$_2$O$_3$@MOF with the magnified image of the surface (d). Cross-sectional TEM images of (e) Nylon@Al$_2$O$_3$ and (f) Nylon@Al$_2$O$_3$@MOF.

precursor and water on the nylon microfiber yielded a 45 nm-thin Al$_2$O$_3$ layer coated on the surface. Notably, there is no discernible morphological difference before and after Al$_2$O$_3$ deposition. The surface of Nylon@Al$_2$O$_3$ (Figure 2b) was as smooth as that of the pristine nylon microfiber (Figures 2a and S1a). However, EDS data revealed the presence of Al only on Nylon@Al$_2$O$_3$ but not on the pristine nylon microfiber (Figure S3 and Table S1).

Following the deposition of Al$_2$O$_3$ on the surface of nylon microfiber, MOFs grew on its surface via a two-step method. In the first step of seeding, the Al$_2$O$_3$ on the surface of microfiber

acted as the aluminum precursor, which reacted with carboxylic acids of NH$_2$-BDC linker under hydrothermal conditions to yield Nylon@Al$_2$O$_3$-BDC.[29] The chemical reaction created a seed layer for uniform MOF growth in the subsequent step. The color of Nylon@Al$_2$O$_3$-BDC changed to dark yellow (Figure 1d), which is the natural color of the organic linker itself. The dark yellow did not fade through a successive wash with water or organic solvent, indicating a tight bound the molecule on the nylon microfiber surface.

Then, MOFs grew on the NH$_2$-BDC seeded microfiber through solvothermal reaction to yield Nylon@Al$_2$O$_3$@MOF. The color of Nylon@Al$_2$O$_3$-BDC changed from yellow to dark brown (Figure 1e), consistent with that of the MIL-101-NH$_2$ powder (Figure S1c), indicating the successful growth of MIL-101-NH$_2$ on the surface. SEM and cross-sectional TEM images clearly showed the growth of MOF crystals on the fiber surface(Figure 2c,d,f). The surface-grown MIL-101-NH$_2$ nanoparticles had octahedral shapes, with average diameters of around 400 nm, similar to that of MIL-101-NH$_2$ powder (Figure S1b). The interface was not smooth, and the average thickness of the MOF layer was around 1.2 μm under the synthetic condition employed.

The XPS spectra reveal show the change in sample components change at each synthetic step (Figure 3a, Table S2). The pristine nylon fiber consists of C, O, and N, as expected. The convoluted C 1s peaks at 284.8, 286.0, and 288.0 eV are attributed to C−C, C−N, and N−C=O, respectively (Figure S4).[40] Following the ALD process, the appearance of Al 2s and Al 2p peaks and the increase of the O 1s peak indicate the formation of Al$_2$O$_3$. The atomic ratio of Al:O, 30.8%: 45.4%, closely approximates that of Al$_2$O$_3$, which is 2:3. The O 1s peak comprises Al−O and Al−OH at 531.0 and 533.0 eV, respectively. The N 1s peak, initially detected in the nylon microfiber, disappeared in Nylon@Al$_2$O$_3$ due to the limited detection depth of XPS, indicating complete coverage of the nylon fiber surface by the Al$_2$O$_3$ layer. After the NH$_2$-BDC seeding process, the N 1s peak appeared again, and the Al 2p peak was significantly reduced to 2.0%.The newly appeared peak at 288.6 eV in high-resolution C 1s peaks corresponds to O=C−O from the carboxyl group in NH$_2$-BDC. Additionally, the O 1s peaks shift from 532.9 eV for Nylon@Al$_2$O$_3$ to 532.0 eV for Nylon@Al$_2$O$_3$-BDC, which consists of C−O/O=C−O and Al−O bonds, indicating chemical bonding of the NH$_2$-BDC linker on the Al$_2$O$_3$ surface. Subsequently, no Al peak was detected on the surface of Nylon@Al$_2$O$_3$@MOF, and the Fe 2p peak appeared after MOF growth. The composition ratio of the Nylon@Al$_2$O$_3$@MOF was nearly identical to that of MOF powder. The Fe 2p high-resolution spectra (Figure S5) show two dominant peaks of MIL-101-NH$_2$ at 711.7 and 725.1 eV indexing to Fe 2p$_{3/2}$ and Fe 2p$_{1/2}$, respectively, with the other two peaks as satellite peaks, analogous to those of the powder itself.[41] After MOF growth, there was no change in C 1s peaks, but new peaks in O 1s appeared at 530.3 and 531.7 eV indexing to Fe−O and Fe−OH from MIL-101-NH$_2$(Fe), respectively.[41] These results support the successful synthesis of MOFs on the nylon microfiber.

Figure 3b shows the FTIR spectra of MOF-coated nylon microfibers at each synthetic step. The nylon microfiber exhibited typical vibration bands at 3300, 2780−3000, 1640, and 1550 cm^{-1}, corresponding to the N−H, C−H, C=O, and C−N stretching vibration from carbonyl and amide groups in nylon, respectively.[42,43] The spectrum of Nylon@Al$_2$O$_3$ showed a broad peak in the range of 800−1000 cm^{-1},
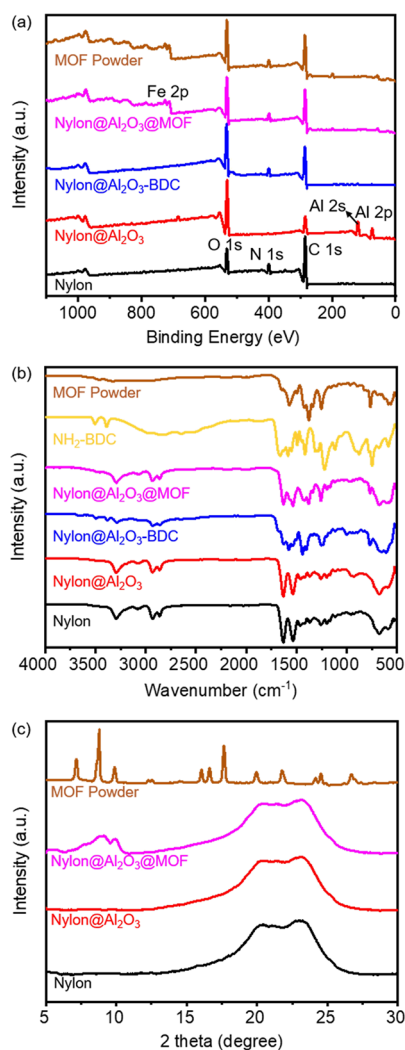
Figure 3. (a) XPS survey, (b) FTIR, and (c) XRD spectra of MOF powder and MOF-coated microfibers at each synthetic step.

pertained to the Al−O−Al phonon mode from the ALD Al_2O_3 layer.[44,45] The characteristic peaks of NH_2-BDC appeared after the seeding process with two bands at 1530−1650 and 1380−1420 cm^{-1} attributed to C=O bonding in the carboxylates and the aromatic carbon C−C vibrational mode, respectively.[46,47] The amine group in NH_2-BDC was observed at 1258 cm^{-1}, corresponding to the C−N stretching attached to the aromatic ring.[46] Small sharp peaks appeared at 3495 and 3382 cm^{-1} can be assigned to symmetric and asymmetric vibration of NH_2, as observed in NH_2-BDC.[48] After MOF growth, the C=O bonding from carboxylic acid at 1666 cm^{-1} disappeared, and C=O bonding from carboxylate became distinctive at 1630 cm^{-1}, which can be attributed to the coordination of the COO− groups with the metallic cations.[48]

In addition, we carried out XRD analyses to confirm the growth of MOFs on nylon microfibers at each synthetic step (Figure 3c). The two broad peaks at around 20.5 and 23.5° correspond to the reflection of (100) and (010, 110) of the α phase of nylon microfiber.[49] After Al_2O_3 ALD, the characteristic peak of Al_2O_3 was not detected, which might be due to the amorphous form of the grown Al_2O_3 under 300 °C and/or the nanometer-thin thickness of the Al_2O_3 layer.[50] After MOF growth on the nylon microfiber, the additional crystalline peaks around 8−10°, corresponding to MIL-101-NH_2 powder,[37]

were detected, along with the broad nylon peaks in Nylon@Al_2O_3@MOF, manifesting the successful synthesis of target MOF structure. The low crystallinity observed in the Nylon@Al_2O_3@MOF sample could be attributed to the low concentration resulting from the very thin film thickness of the MOF (1.2 μm).

TGA was employed to determine the loading amount of MOF on nylon fibers (Figure 4). The TGA curve of pure
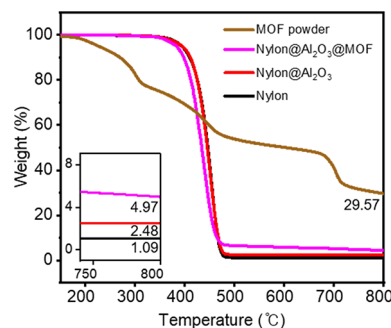

Figure 4. TGA curves of a nylon microfiber, Nylon@Al_2O_3, Nylon@Al_2O_3@MOF, and MOF powder. The inset is the magnified graph for the clarification of residue amount.

nylon fiber showed significant weight loss at ca. 350−490 °C, which is attributed to the thermal degradation of nylon. The residue of nylon at 800 °C was only 1.09%. Similarly, Nylon@Al_2O_3 exhibited thermal degradation at 350−490 °C with the residue at 800 °C of 2.48%. The difference in residual amounts between the nylon fiber and Nylon@Al_2O_3 was attributed to the Al_2O_3 layer. The residues of Nylon@Al_2O_3@MOF and MOF powder at 800 °C were 4.97 and 29.57%, respectively. The growth of MOFs on fiber contributed to the increase of the residue at 800 °C. Based on these results, the loading of MIL-101-NH_2 in Nylon@Al_2O_3@MOF was calculated to be 9.2 wt % (see SI for the calculation).

Control experiments were conducted to investigate the impact of the metal oxide adhesion layer and organic linker layer on the adhesion of MOF crystals, in which MOF-grown microfiber samples were fabricated without the Al_2O_3 ALD process (Nylon@MOF) and seeding processes (Nylon@Al_2O_3@MOF_no seeding). SEM images revealed sparsely attached MOF crystals in both Nylon@MOF and Nylon@Al_2O_3@MOF_no seeding (Figure S6), with bundles of MOF crystals adhering to the surface in the no seeding sample rather than uniform growth as observed in Nylon@Al_2O_3@MOF. TGA results also show the difference in MOF loading in these samples (Figure S7). The residues of Nylon@MOF and Nylon@Al_2O_3@MOF_no seeding at 800 °C were 1.43 and 3.11%, respectively. The loadings of MIL-101-NH_2 on each sample were calculated to 1.2 and 2.3 wt %, which are way below 9.2 wt % of Nylon@Al_2O_3@MOF. These findings suggest that the Al_2O_3-ALD and BDC-seeding processes are crucial for achieving a tight bond between MIL-101-NH_2 crystals and the surface of the nylon fiber.

The Al_2O_3-ALD provided metal (Al) sites on the nylon fiber surface that could react with the NH_2-BDC linker. Furthermore, NH_2-BDC on the surface of nylon fiber, formed through the seeding process, facilitated surface-initiated growth of MOFs. Nylon@MOF, which lacked Al sites on its surface, exhibited the weakest MOF growth. In this case, NH_2-BDC was unable to react with the surface of pure nylon fiber during

the seeding process, thus inhibiting surface-initiated MOF growth in the later stages. In contrast, Nylon@Al$_2$O$_3$@MOF_no seeding showed better MOF surface growth than Nylon@MOF but worse than Nylon@Al$_2$O$_3$@MOF with the seeding process. During the solvothermal synthesis of MOFs, the majority of NH$_2$-BDC reacted with the free Fe precursor in the reaction solution, with only a small amount bonding to the underlaid Al sites on the surface, resulting in a bundle of MOF islands on the surface (Figure S6b).

We evaluated the photocatalytic performances of MOF-coated nylon microfibers and MIL-101-NH$_2$ powder by investigating the degradation study of RhB and Cr(VI) aqueous solution (Figures 5, S8, and S9, Tables S3−S5). As
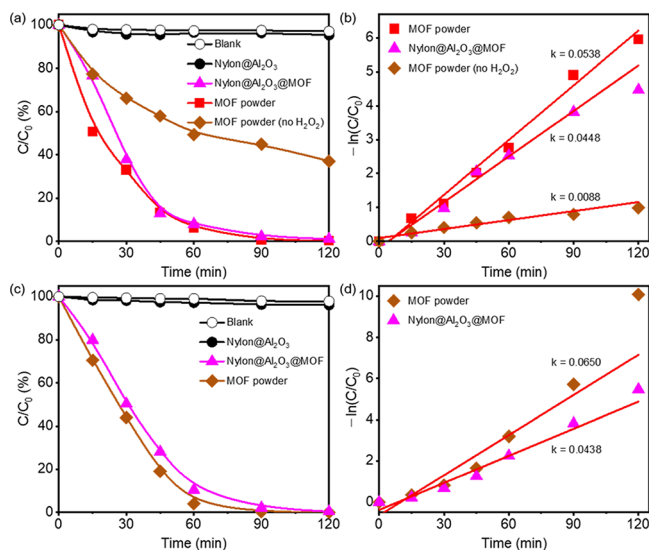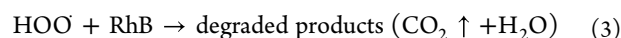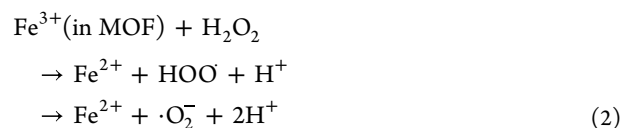

Figure 5. Photocatalytic degradation of RhB and Cr(VI) over the samples under white light irradiation condition: (1) RhB, 60 mL of 50 mg/L RhB, 15 mg of MOF powder, 1 g of fiber samples, 1.5 mL of 35% H$_2$O$_2$, and pH 8; (2) Cr(VI), 60 mL of 10 mg/L Cr(VI), 15 mg of MOF powder, 1 g of fiber samples, and pH 2. (a and c) C/C$_0$ vs time plots. (b and d) −ln(C/C$_0$) vs time plots.

shown in Figure 5a,c, the concentration of both solutions remained unchanged in the absence of photocatalysts. However, with the addition of 15 mg of MOF powder, the concentration of RhB and Cr(VI) solution decreased by 24.0 and 14.0%, respectively, after 1 h of stirring, to reach adsorption/desorption equilibrium. After 2 h of light irradiation, each concentration decreased by 62.9% (RhB) and 100.0% (Cr(VI)) from the equilibrium concentration, respectively. We also found that the addition of H$_2$O$_2$ as an oxidant in the Fenton-like reaction[51,52] accelerated the degradation of RhB solution to 99.7% in 2 h of light irradiation. The concentration changes under light irradiation were fitted well by the pseudo-first-order rate expressions. The rate constant k was calculated to 0.0538 min^{-1} for RhB degradation with H$_2$O$_2$ and 0.065 min^{-1} for Cr(VI) reduction. Here, the calculation was performed within the range between 0 and 90 min, which achieved over 99% degradation.

Subsequently, we conducted degradation experiments with Nylon@Al$_2$O$_3$ and Nylon@Al$_2$O$_3$@MOF (Tables S6−S9). The addition of 1 g of Nylon@Al$_2$O$_3$ resulted in a light decrease in the concentrations of RhB and Cr(VI) solutions, approximately 4.5%, due to adsorption in the dark state. However, Nylon@Al$_2$O$_3$ exhibited almost no distinctive

photocatalytic activities with less than 5% degradation within 2 h. Upon adding 1 g of Nylon@Al$_2$O$_3$@MOF to the aqueous solution, the adsorption-induced concentration change increased to 12.6% for RhB and 10.0% for Cr(VI), respectively, which are smaller than those of MOF powders themselves. After 2 h of light irradiation, the concentration of RhB solution with H$_2$O$_2$ decreased by 98.9%, and the concentration of Cr(VI) solution decreased by 99.6%. These results are comparable to other MIL-101-NH$_2$ systems (Tables S10 and S11). The rate constants k were 0.0448 min^{-1} for RhB and 0.0438 min^{-1} for Cr(VI) degradation, respectively. When considering the actual amount of MOF in the powder catalyst and MOF-coated fiber, the difference is more dramatic. One gram of Nylon@Al$_2$O$_3$@MOF contains 92 mg of MIL-101-NH$_2$, based on the TGA result above. The degradation rate constants per the amount of catalyst were 3.59 and 0.49 min^{-1} g^{-1} for MOF powder and Nylon@Al$_2$O$_3$@MOF in the RhB degradation experiment, respectively. These findings suggest that the catalytically active MOF in Nylon@Al$_2$O$_3$@MOF is located only at a few depths from the outmost surface. Moreover, a comparison of the adsorption-induced concentration between MOF powder (15 mg, 24.0%) and Nylon@Al$_2$O$_3$@MOF (1 g, 12.6%) indicates that only 7.9 mg of MIL-101-NH$_2$ within Nylon@Al$_2$O$_3$@MOF adsorbs RhB molecules. It was assumed that the free MOF nanocrystal is small enough for the RhB molecule to easily permeate the entire crystal without leaving any untouched inside space. RhB was found to penetrate only about 8.6 wt % of the total MOF (92 mg) from the surface of the Nylon@Al$_2$O$_3$@MOF. In such a thick layer (∼1.2 μm) of MOF on nylon microfiber (Figure 2f), only the top surface of the MOF was found to exhibit catalytic activity. These results suggest that thinning the MOF layer would increase the catalytic activity per mass in MOF-coated fibers.

Moreover, we examined the effect of pH on degradation efficiency. The photocatalytic activity in the RhB solution improved with an increase in pH, while the performance in Cr(VI) solution deteriorated (Figure 6). On the basis of the literature, RhB degradation with Fe-based MOFs and H$_2$O$_2$ involves a Fenton-like reaction mechanism.[52,53] In short, H$_2$O$_2$ reduces Fe(III) in the catalyst to Fe(II), producing HOO· and ·O$_2^-$ (eqs 2 and 3, Scheme S1). Subsequently, the active radical reacts with the adsorbed dye to promote degradation. Under basic conditions, the production of H$^+$ accelerates the formation of active species.

$$\text{Fe}^{3+}(\text{in MOF}) + \text{H}_2\text{O}_2$$
$$\rightarrow \text{Fe}^{2+} + \text{HOO}\cdot + \text{H}^+$$
$$\rightarrow \text{Fe}^{2+} + \cdot\text{O}_2^- + 2\text{H}^+ \tag{2}$$

$$\text{HOO}\cdot + \text{RhB} \rightarrow \text{degraded products (CO}_2 \uparrow + \text{H}_2\text{O}) \tag{3}$$

The reduction of hexavalent chromium by MIL-101-NH$_2$(Fe) in an acidic environment follows eqs 4 and 5, where photo-excited electrons from the MOFs and excess H$^+$ facilitate the reduction of Cr(VI) to Cr(III).[30] On the other hand, the majority of Cr(VI) exists in the form of CrO$_4^{2-}$ in an alkaline environment. During the reduction of CrO$_4^{2-}$ (eq 6), the produced Cr(OH)$_3$ precipitates on the catalyst surface, resulting in the deterioration of catalytic performance.
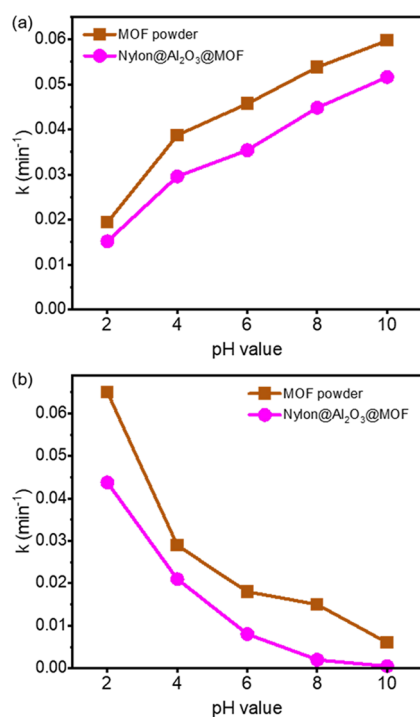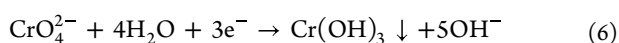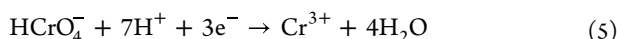
$$\text{Cr}_2\text{O}_7^{2-} + 14\text{H}^+ + 6e^- \rightarrow 2\text{Cr}^{3+} + 7\text{H}_2\text{O} \tag{4}$$

Figure 6. Effect of solution pH on photocatalytic degradation of (a) RhB and (b) Cr(VI) over Nylon@Al$_2$O$_3$@MOF and MOF powder.

$$HCrO_4^- + 7H^+ + 3e^- \rightarrow Cr^{3+} + 4H_2O \qquad (5)$$

$$CrO_4^{2-} + 4H_2O + 3e^- \rightarrow Cr(OH)_3 \downarrow + 5OH^- \qquad (6)$$

The reusability of catalysts is essential for practical application. To assess the reusability, we conducted recycling tests of Nylon@Al$_2$O$_3$@MOF. Nylon@Al$_2$O$_3$@MOF retained its photocatalytic activities over 85% for five cycles in both RhB and Cr(VI) degradation experiments (Figure 7a). The decrease in catalytic activity might be attributed to the weight loss induced by the detachment of the nanocrystals during solution stirring. However, this weight loss was significantly less than that observed in powder catalysis, where most of the catalyst is lost during centrifugation or filtration. In contrast, MOF-coated fiber can be readily removed from the liquid phase and reused with a simple wash process. TGA analysis showed that the residue of the five-cycled Nylon@Al$_2$O$_3$@MOF was 4.68% at 800 °C (Figure S10). The loading of MIL-101-NH$_2$ in the five-cycled Nylon@Al$_2$O$_3$@MOF was calculated to 8.1 wt %, which closely corresponded to the reduction in catalytic activity (Figure 7a). The observed reduction in MIL-101-NH$_2$ loading could be attributed to the weaker binding of the MOF through physisorption in the outmost layer, in contrast to the chemical bonding of the initial layers of MOF on the microfiber substrate, as illustrated in Figure 1a. However, since only the top surface of the MOF layer was found to exhibit catalytic activity, it is reasonable to attribute the reduction of photocatalytic activity in multiple use to the potential catalyst poisoning[54−56] from H$_2$O$_2$, dye molecules and hydrocarbons. Additionally, the XRD patterns and SEM images of the recovered Nylon@Al$_2$O$_3$@MOF were almost identical to those of the fresh sample (Figure 7b,c). Overall, these results demonstrate that Nylon@Al$_2$O$_3$@MOF is a highly stable and reusable photocatalyst for the degradation of organic and inorganic pollutants in water.
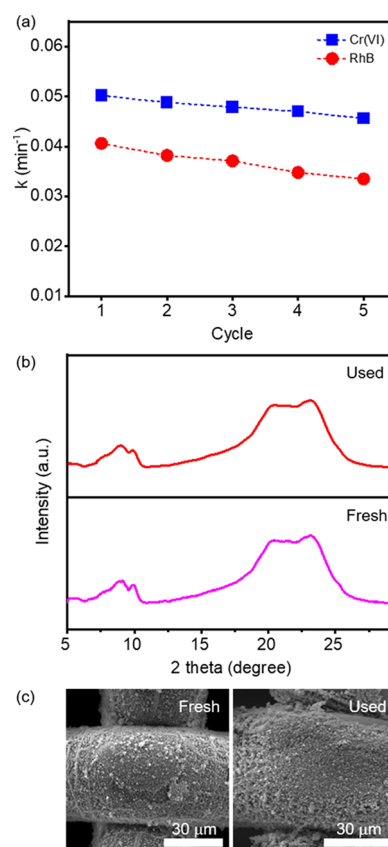

Figure 7. Reusability test of RhB degradation and Cr(VI) reduction over Nylon@Al$_2$O$_3$@MOF under white light irradiation. (a) Rate constant vs cycles. (b) XRD patterns and (c) SEM images of fresh and five cycled-Nylon@Al$_2$O$_3$@MOF.

■ CONCLUSIONS

In this study, we successfully prepared a MOF-coated nylon microfiber through Al$_2$O$_3$ ALD and the two-step synthesis of MIL-101-NH$_2$(Fe). The Al$_2$O$_3$ layer and NH$_2$-BDC linkers were crucial for the uniform growth of the MOF on the microfiber mesh. The Al$_2$O$_3$ layer provided metal sites on the nylon fiber surface for NH$_2$-BDC to coordinate in the successive seeding process, while NH$_2$-BDC facilitated surface-initiated MOF growth. Then, we evaluated the photocatalytic performance of the fiber-immobilized MOF for the RhB and Cr(VI) removal. Although the catalytic efficiency of the fiber-immobilized MOFs was lower than powder-formed MOFs, their superior recyclability makes them a more practical choice for photocatalytic applications. The proposed method for preparing nanoparticle-coated microfibers has potential for the development of various types of heterogeneous catalysts.

■ ASSOCIATED CONTENT

Ⓢ Supporting Information

The Supporting Information is available free of charge at https://pubs.acs.org/doi/10.1021/acsomega.3c00432.

SEM images; illustration of photocatalytic reaction; EDS data; atomic percent of a nylon microfiber and Nylon@Al$_2$O$_3$ from EDS data; atomic percent of each step sample from XPS measurements; high-resolution *C 1s*, *O 1s*, and *Fe 2p* XPS spectra; TGA data; photocatalytic degradation of RhB and Cr(VI); illustration of proposed photocatalytic mechanisms; detailed reaction pathway of

RhB degradation; photocatalytic removal of RhB and Cr(VI) using MOF-based catalyst; TGA curves of the fresh- and used-Nylon@Al$_2$O$_3$@MOF (PDF)

■ AUTHOR INFORMATION

Corresponding Author

Sangho Cho − *Materials Architecturing Research Center, Korea Institute of Science and Technology, Seoul 02792, Republic of Korea; Division of Nano and Information Technology, KIST School, Korea University of Science and Technology, Seoul 02792, Republic of Korea;* ◉ orcid.org/0000-0002-9627-5310; Email: scho@kist.re.kr

Authors

Munchan Kang − *Materials Architecturing Research Center, Korea Institute of Science and Technology, Seoul 02792, Republic of Korea; Department of Chemistry, Hanyang University, Seoul 04763, Republic of Korea;* Present Address: LG Display, 245, LG-ro, Wollong-myeon, Paju-si, Gyeonggi-do 10845, Republic of Korea

Sung Ho Yu − *Materials Architecturing Research Center, Korea Institute of Science and Technology, Seoul 02792, Republic of Korea; Department of Chemistry, Hanyang University, Seoul 04763, Republic of Korea*

Kyung-Youl Baek − *Materials Architecturing Research Center, Korea Institute of Science and Technology, Seoul 02792, Republic of Korea; Division of Nano and Information Technology, KIST School, Korea University of Science and Technology, Seoul 02792, Republic of Korea; KHU-KIST Department of Converging Science and Technology, Kyung Hee University, Seoul 02447, Republic of Korea;* ◉ orcid.org/0000-0002-8106-2849

Myung Mo Sung − *Department of Chemistry, Hanyang University, Seoul 04763, Republic of Korea;* ◉ orcid.org/0000-0002-2291-5274

Complete contact information is available at:
https://pubs.acs.org/10.1021/acsomega.3c00432

Notes

The authors declare no competing financial interest.

■ REFERENCES

(1) Geissen, V.; Mol, H.; Klumpp, E.; Umlauf, G.; Nadal, M.; van der Ploeg, M.; van de Zee, S. E. A. T. M.; Ritsema, C. J. Emerging pollutants in the environment: A challenge for water resource management. *Int. Soil Water Conserv. Res.* **2015**, *3*, 57−65.

(2) Zhao, Z.; An, H.; Lin, J.; Feng, M.; Murugadoss, V.; Ding, T.; Liu, H.; Shao, Q.; Mai, X.; Wang, N.; Gu, H.; Angaiah, S.; Guo, Z. Progress on the Photocatalytic Reduction Removal of Chromium Contamination. *Chem. Rec.* **2019**, *19*, 873−882.

(3) Vardhan, K. H.; Kumar, P. S.; Panda, R. C. A review on heavy metal pollution, toxicity and remedial measures: Current trends and future perspectives. *J. Mol. Liq.* **2019**, *290*, No. 111197.

(4) Pakade, V. E.; Tavengwa, N. T.; Madikizela, L. M. Recent advances in hexavalent chromium removal from aqueous solutions by adsorptive methods. *RSC Adv.* **2019**, *9*, 26142−26164.

(5) Peng, H.; Guo, J. Removal of chromium from wastewater by membrane filtration, chemical precipitation, ion exchange, adsorption electrocoagulation, electrochemical reduction, electrodialysis, electro-deionization, photocatalysis and nanotechnology: a review. *Environ. Chem. Lett.* **2020**, *18*, 2055−2068.

(6) Loeb, S. K.; Alvarez, P. J. J.; Brame, J. A.; Cates, E. L.; Choi, W.; Crittenden, J.; Dionysiou, D. D.; Li, Q.; Li-Puma, G.; Quan, X.; Sedlak, D. L.; David Waite, T.; Westerhoff, P.; Kim, J.-H. The Technology Horizon for Photocatalytic Water Treatment: Sunrise or Sunset? *Environ. Sci. Technol.* **2019**, *53*, 2937−2947.

(7) Rehman, S.; Ullah, R.; Butt, A. M.; Gohar, N. D. Strategies of making TiO2 and ZnO visible light active. *J. Hazard. Mater.* **2009**, *170*, 560−569.

(8) Chen, D.; Ray, K. A. Removal of toxic metal ions from wastewater by semiconductor photocatalysis. *Chem. Eng. Sci.* **2001**, *56*, 1561−1570.

(9) Shekhah, O.; Liu, J.; Fischer, R. A.; Wöll, C. MOF thin films: existing and future applications. *Chem. Soc. Rev.* **2011**, *40*, 1081−1106.

(10) Ding, M.; Cai, X.; Jiang, H.-L. Improving MOF stability: approaches and applications. *Chem. Sci.* **2019**, *10*, 10209−10230.

(11) Alkhatib, I. I.; Garlisi, C.; Pagliaro, M.; Al-Ali, K.; Palmisano, G. Metal-organic frameworks for photocatalytic CO2 reduction under visible radiation: A review of strategies and applications. *Catal. Today* **2020**, *340*, 209−224.

(12) Jafarzadeh, M. Recent Progress in the Development of MOF-Based Photocatalysts for the Photoreduction of Cr(VI). *ACS Appl. Mater. Interfaces* **2022**, *14*, 24993−25024.

(13) Guo, M.; Zhang, M.; Liu, R.; Zhang, X.; Li, G. State-of-the-Art Advancements in Photocatalytic Hydrogenation: Reaction Mechanism and Recent Progress in Metal-Organic Framework (MOF)-Based Catalysts. *Adv. Sci.* **2022**, *9*, No. 2103361.

(14) Ramsahye, N. A.; Trung, T. K.; Scott, L.; Nouar, F.; Devic, T.; Horcajada, P.; Magnier, E.; David, O.; Serre, C.; Trens, P. Impact of the Flexible Character of MIL-88 Iron(III) Dicarboxylates on the Adsorption of n-Alkanes. *Chem. Mater.* **2013**, *25*, 479−488.

(15) Xia, Q.; Wang, H.; Huang, B.; Yuan, X.; Zhang, J.; Zhang, J.; Jiang, L.; Xiong, T.; Zeng, G. State-of-the-Art Advances and Challenges of Iron-Based Metal Organic Frameworks from Attractive Features, Synthesis to Multifunctional Applications. *Small* **2019**, *15*, No. 1803088.

(16) Laurier, K. G. M.; Vermoortele, F.; Ameloot, R.; De Vos, D. E.; Hofkens, J.; Roeffaers, M. B. J. Iron(III)-Based Metal−Organic Frameworks As Visible Light Photocatalysts. *J. Am. Chem. Soc.* **2013**, *135*, 14488−14491.

(17) Zhang, M.-W.; Lin, K.-Y. A.; Huang, C.-F.; Tong, S. Enhanced degradation of toxic azo dye, amaranth, in water using Oxone catalyzed by MIL-101-NH2 under visible light irradiation. *Sep. Purif. Technol.* **2019**, *227*, No. 115632.

(18) Du, X.-D.; Yi, X.-H.; Wang, P.; Zheng, W.; Deng, J.; Wang, C.-C. Robust photocatalytic reduction of Cr(VI) on UiO-66-NH2(Zr/Hf) metal-organic framework membrane under sunlight irradiation. *Chem. Eng. J.* **2019**, *356*, 393−399.

(19) Yi, X.-H.; Ma, S.-Q.; Du, X.-D.; Zhao, C.; Fu, H.; Wang, P.; Wang, C.-C. The facile fabrication of 2D/3D Z-scheme g-C3N4/UiO-66 heterojunction with enhanced photocatalytic Cr(VI) reduction performance under white light. *Chem. Eng. J.* **2019**, *375*, No. 121944.

(20) Rao, K. V. S.; Subrahmanyam, M.; Boule, P. Immobilized TiO2 photocatalyst during long-term use: decrease of its activity. *Appl. Catal. B Environ.* **2004**, *49*, 239−249.

(21) Carlson, P. J.; Pretzer, L. A.; Boyd, J. E. Solvent Deposition of Titanium Dioxide on Acrylic for Photocatalytic Application. *Ind. Eng. Chem. Res.* **2007**, *46*, 7970−7976.

(22) Donnadio, A.; Narducci, R.; Casciola, M.; Marmottini, F.; D'Amato, R.; Jazestani, M.; Chiniforoshan, H.; Costantino, F. Mixed

Membrane Matrices Based on Nafion/UiO-66/SO3H-UiO-66 Nano-MOFs: Revealing the Effect of Crystal Size, Sulfonation, and Filler Loading on the Mechanical and Conductivity Properties. *ACS Appl. Mater. Interfaces* **2017**, *9*, 42239–42246.

(23) Song, Y.; Seo, J. Y.; Kim, H.; Cho, S.; Baek, K.-Y. Pore-size control of chitin nanofibrous composite membrane using metal-organic frameworks. *Carbohydr. Polym.* **2022**, *275*, No. 118754.

(24) Seo, J. Y.; Choi, M. H.; Lee, B. W.; Lee, J.-H.; Shin, S.; Cho, S.; Cho, K. Y.; Baek, K.-Y. Feasible Detoxification Coating Material for Chemical Warfare Agents Using Poly(methyl methacrylate)−Branched Poly(ethyleneimine) Copolymer and Metal−Organic Framework Composites. *ACS Appl. Mater. Interfaces* **2022**, *14*, 50246–50255.

(25) Liu, T.-Y.; Yuan, H.-G.; Liu, Y.-Y.; Ren, D.; Su, Y.-C.; Wang, X. Metal−Organic Framework Nanocomposite Thin Films with Interfacial Bindings and Self-Standing Robustness for High Water Flux and Enhanced Ion Selectivity. *ACS Nano* **2018**, *12*, 9253–9265.

(26) Mukhopadhyay, S.; Das, A.; Jana, T.; Das, S. K. Fabricating a MOF Material with Polybenzimidazole into an Efficient Proton Exchange Membrane. *ACS Appl. Energy Mater.* **2020**, *3*, 7964–7977.

(27) Fouad, K.; Bassyouni, M.; Alalm, M. G.; Saleh, M. Y. Recent developments in recalcitrant organic pollutants degradation using immobilized photocatalysts. *Appl. Phys. A: Mater. Sci. Process.* **2021**, *127*, 612.

(28) Liao, W.; Zhao, M.; Rong, H.; Jiang, P.; Liao, Q.; Zhang, C.; Chen, Y. Photocatalyst immobilized by hydrogel, efficient degradation and self regeneration: A review. *Mater. Sci. Semicond. Process.* **2022**, *150*, No. 106929.

(29) Hu, Y.; Dong, X.; Nan, J.; Jin, W.; Ren, X.; Xu, N.; Lee, Y. M. Metal−organic framework membranes fabricated via reactive seeding. *Chem. Commun.* **2011**, *47*, 737–739.

(30) Zhao, Q.; Yi, X.-H.; Wang, C.-C.; Wang, P.; Zheng, W. Photocatalytic Cr(VI) reduction over MIL-101(Fe)−NH2 immobilized on alumina substrate: From batch test to continuous operation. *Chem. Eng. J.* **2022**, *429*, No. 132497.

(31) Leskelä, M.; Ritala, M. Atomic Layer Deposition Chemistry: Recent Developments and Future Challenges. *Angew. Chem., Int. Ed.* **2003**, *42*, 5548–5554.

(32) Knez, M.; Nielsch, K.; Niinistö, L. Synthesis and Surface Engineering of Complex Nanostructures by Atomic Layer Deposition. *Adv. Mater.* **2007**, *19*, 3425–3438.

(33) Lee, L.; Yoon, K. H.; Jung, J. W.; Yoon, H. R.; Kim, H.; Kim, S. H.; Song, S. Y.; Park, K. S.; Sung, M. M. Ultra Gas-Proof Polymer Hybrid Thin Layer. *Nano Lett.* **2018**, *18*, 5461–5466.

(34) Park, J.; Yoon, H. R.; Khan, M. A.; Cho, S.; Sung, M. M. Selective Infiltration in Polymer Hybrid Thin Films as a Gas-Encapsulation Layer for Stretchable Electronics. *ACS Appl. Mater. Interfaces* **2020**, *12*, 8817–8825.

(35) Bulusu, A.; Graham, S.; Bahre, H.; Behm, H.; Böke, M.; Dahlmann, R.; Hopmann, C.; Winter, J. The Mechanical Behavior of ALD-Polymer Hybrid Films Under Tensile Strain. *Adv. Eng. Mater.* **2015**, *17*, 1057–1067.

(36) Saini, S.; Chakraborty, D.; Erakulan, E. S.; Thapa, R.; Bal, R.; Bhaumik, A.; Jain, S. L. Visible Light-Driven Metal−Organic Framework-Mediated Activation and Utilization of CO2 for the Thiocarboxylation of Olefins. *ACS Appl. Mater. Interfaces* **2022**, *14*, 50913–50922.

(37) Bauer, S.; Serre, C.; Devic, T.; Horcajada, P.; Marrot, J.; Férey, G.; Stock, N. High-Throughput Assisted Rationalization of the Formation of Metal Organic Frameworks in the Iron(III) Amino-terephthalate Solvothermal System. *Inorg. Chem.* **2008**, *47*, 7568–7576.

(38) Han, G.; Rodriguez, K. M.; Qian, Q.; Smith, Z. P. Acid-Modulated Synthesis of High Surface Area Amine-Functionalized MIL-101(Cr) Nanoparticles for CO2 Separations. *Ind. Eng. Chem. Res.* **2020**, *59*, 18139–18150.

(39) Gardner, M.; Comber, S. Determination of trace concentrations of hexavalent chromium. *Analyst* **2002**, *127*, 153–156.

(40) Nascimento, L.; Gasi, F.; Landers, R.; da Silva Sobrinho, A.; Aragão, E.; Fraga, M.; Petraconi, G.; Chiappim, W.; Pessoa, R. Physicochemical Studies on the Surface of Polyamide 6.6 Fabrics Functionalized by DBD Plasmas Operated at Atmospheric and Sub-Atmospheric Pressures. *Polymer* **2020**, *12*, 2128.

(41) Liu, J.; Hao, D.; Sun, H.; Li, Y.; Han, J.; Fu, B.; Zhou, J. Integration of MIL-101-NH2 into Cellulosic Foams for Efficient Cr(VI) Reduction under Visible Light. *Ind. Eng. Chem. Res.* **2021**, *60*, 12220–12227.

(42) Shao, H.-I.; Umemoto, S.; Kikutani, T.; Okui, N. Layer-by-layer polycondensation of nylon 66 by alternating vapour deposition polymerization. *Polymer* **1997**, *38*, 459–462.

(43) Du, Y.; George, S. M. Molecular Layer Deposition of Nylon 66 Films Examined Using in Situ FTIR Spectroscopy. *J. Phys. Chem. C* **2007**, *111*, 8509–8517.

(44) Goldstein, D. N.; McCormick, J. A.; George, S. M. Al2O3 Atomic Layer Deposition with Trimethylaluminum and Ozone Studied by in Situ Transmission FTIR Spectroscopy and Quadrupole Mass Spectrometry. *J. Phys. Chem. C* **2008**, *112*, 19530–19539.

(45) Koushik, D.; Hazendonk, L.; Zardetto, V.; Vandalon, V.; Verheijen, M. A.; Kessels, W. M. M.; Creatore, M. Chemical Analysis of the Interface between Hybrid Organic−Inorganic Perovskite and Atomic Layer Deposited Al2O3. *ACS Appl. Mater. Interfaces* **2019**, *11*, 5526–5535.

(46) Kandiah, M.; Usseglio, S.; Svelle, S.; Olsbye, U.; Lillerud, K. P.; Tilset, M. Post-synthetic modification of the metal−organic framework compound UiO-66. *J. Mater. Chem.* **2010**, *20*, 9848–9851.

(47) Xie, Q.; Li, Y.; Lv, Z.; Zhou, H.; Yang, X.; Chen, J.; Guo, H. Effective Adsorption and Removal of Phosphate from Aqueous Solutions and Eutrophic Water by Fe-based MOFs of MIL-101. *Sci. Rep.* **2017**, *7*, 3316.

(48) Kalhor, S.; Zarei, M.; Zolfigol, M. A.; Sepehrmansourie, H.; Nematollahi, D.; Alizadeh, S.; Shi, H.; Arjomandi, J. Anodic electrosynthesis of MIL-53(Al)-N(CH2PO3H2)2 as a mesoporous catalyst for synthesis of novel (N-methyl-pyrrol)-pyrazolo[3,4-b]-pyridines via a cooperative vinylogous anomeric based oxidation. *Sci. Rep.* **2021**, *11*, 19370.

(49) Billon, N.; Giraudeau, J.; Bouvard, J. L.; Robert, G. Mechanical Behavior−Microstructure Relationships in Injection-Molded Poly-amide 66. *Polymers* **2018**, *10*, 1047.

(50) Miikkulainen, V.; Leskelä, M.; Ritala, M.; Puurunen, R. L. Crystallinity of inorganic films grown by atomic layer deposition: Overview and general trends. *J. Appl. Phys.* **2013**, *113*, No. 021301.

(51) Zhao, G.; Wang, Y.; Wang, C.; Lei, H.; Yi, B.; Tong, R. Fenton-like chemistry enables catalytic oxidative desulfurization of thioacetals and thioketals with hydrogen peroxide. *Green Chem.* **2022**, *24*, 4041–4049.

(52) Taha, A. A.; Huang, L.; Ramakrishna, S.; Liu, Y. MOF [NH2-MIL-101(Fe)] as a powerful and reusable Fenton-like catalyst. *J. Water Process. Eng.* **2020**, *33*, No. 101004.

(53) Zhang, Z.; Li, X.; Liu, B.; Zhao, Q.; Chen, G. Hexagonal microspindle of NH2-MIL-101(Fe) metal−organic frameworks with visible-light-induced photocatalytic activity for the degradation of toluene. *RSC Adv.* **2016**, *6*, 4289–4295.

(54) Shi, W.; Guo, F.; Wang, H.; Guo, S.; Li, H.; Zhou, Y.; Zhu, C.; Liu, Y.; Huang, H.; Mao, B.; Liu, Y.; Kang, Z. New Insight of Water-Splitting Photocatalyst: H2O2-Resistance Poisoning and Photo-thermal Deactivation in Sub-micrometer CoO Octahedrons. *ACS Appl. Mater. Interfaces* **2017**, *9*, 20585–20593.

(55) Ranjith, K. S.; Rajendra Kumar, R. T. Regeneration of an efficient, solar active hierarchical ZnO flower photocatalyst for repeatable usage: controlled desorption of poisoned species from active catalytic sites. *RSC Adv.* **2017**, *7*, 4983–4992.

(56) Dhakshinamoorthy, A.; Asiri, A. M.; García, H. Metal−Organic Framework (MOF) Compounds: Photocatalysts for Redox Reactions and Solar Fuel Production. *Angew. Chem., Int. Ed.* **2016**, *55*, 5414–5445.